ALZHEIMER'S DISEASE

Prospective longitudinal atrophy in Alzheimer's disease correlates with the intensity and topography of baseline tau-PET

Renaud La Joie[1]*, Adrienne V. Visani[1], Suzanne L. Baker[2], Jesse A. Brown[1], Viktoriya Bourakova[1], Jungho Cha[1], Kiran Chaudhary[1], Lauren Edwards[1], Leonardo Iaccarino[1], Mustafa Janabi[2], Orit H. Lesman-Segev[1], Zachary A. Miller[1], David C. Perry[1], James P. O'Neil[2], Julie Pham[1], Julio C. Rojas[1], Howard J. Rosen[1], William W. Seeley[1], Richard M. Tsai[1], Bruce L. Miller[1], William J. Jagust[2,3], Gil D. Rabinovici[1,2,3,4]

β-Amyloid plaques and tau-containing neurofibrillary tangles are the two neuropathological hallmarks of Alzheimer's disease (AD) and are thought to play crucial roles in a neurodegenerative cascade leading to dementia. Both lesions can now be visualized in vivo using positron emission tomography (PET) radiotracers, opening new opportunities to study disease mechanisms and improve patients' diagnostic and prognostic evaluation. In a group of 32 patients at early symptomatic AD stages, we tested whether β-amyloid and tau-PET could predict subsequent brain atrophy measured using longitudinal magnetic resonance imaging acquired at the time of PET and 15 months later. Quantitative analyses showed that the global intensity of tau-PET, but not β-amyloid–PET, signal predicted the rate of subsequent atrophy, independent of baseline cortical thickness. Additional investigations demonstrated that the specific distribution of tau-PET signal was a strong indicator of the topography of future atrophy at the single patient level and that the relationship between baseline tau-PET and subsequent atrophy was particularly strong in younger patients. These data support disease models in which tau pathology is a major driver of local neurodegeneration and highlight the relevance of tau-PET as a precision medicine tool to help predict individual patient's progression and design future clinical trials.

INTRODUCTION

Alzheimer's disease (AD) is characterized by the co-occurrence of β-amyloid (Aβ) deposition into extracellular plaques and neurofibrillary tangles composed of aggregated hyperphosphorylated tau (*1*). The aggregation of Aβ and tau is thought to play a crucial role in a neurodegenerative cascade that results in the loss of neurons and synapses (*2*). The development of radiotracers binding to Aβ plaques (*3*) and paired helical filaments of tau that comprise neurofibrillary tangles (*4*) allows the visualization and quantification of AD pathology in living patients using positron emission tomography (PET). Those imaging biomarkers offer an opportunity to improve patient diagnosis and to study the development of AD pathophysiology by describing the relationships between protein aggregation, neurodegeneration, and cognitive impairment.

Cross-sectional neuroimaging studies have demonstrated that lower brain volumes are more strongly associated with tau-PET than with Aβ-PET burden in patients with mild cognitive impairment and dementia (*5*). Moreover, studies examining the topography of neuroimaging biomarkers have indicated that the pattern of neurodegeneration [i.e., regions with low cortical volume/thickness (*6*, *7*) or glucose hypometabolism (*8*, *9*)] greatly resembles the pattern of elevated tau-PET, but not Aβ-PET, signal. However, the spatial extent of tau-PET signal appears to exceed the extent of neurodegeneration (*6*, *8*), suggesting that tau-PET elevation might precede and potentially predict neurodegeneration. Converging evidence also suggests that the intensity and topography of tau-PET, but not Aβ-PET, are strongly associated with the severity of each patient's specific clinical deficits (*10*). In addition, earlier age of onset seems to be associated with higher tau-PET signal (*8*, *11*), potentially accounting for the higher rates of brain atrophy observed in patients with early-onset AD compared to their older counterparts (*12*–*14*).

Because tau-PET imaging is a relatively novel technique, most previous studies have been based on cross-sectional data, which lead to technical and conceptual limitations. First, cross-sectional studies define neurodegeneration as low volume/metabolism because they cannot directly measure decline in volume/metabolism over time. Resulting metrics are then biased by preexisting interindividual variability in cerebral anatomy and function (*15*). Second, cross-sectional designs do not allow direct observation of a chronological sequence of biomarker abnormalities. More recently, retrospective longitudinal studies [in which longitudinal magnetic resonance imaging (MRI) data were acquired before tau-PET acquisition] have also highlighted a close association between tau-PET and neurodegeneration (*16*, *17*) but might be biased by the nonlinear nature of atrophy over the disease course (*18*, *19*).

In the present observational study, we prospectively assessed and compared the associations between baseline Aβ and tau-PET burden [using [^{11}C]Pittsburgh compound B (PIB) and [^{18}F]flortaucipir (FTP), respectively] and subsequent longitudinal atrophy in a group of patients at the early clinical stages of AD. Our primary hypothesis was that the tau deposition detected with FTP-PET drives, and therefore precedes, regional neurodegeneration in early symptomatic AD. From a precision medicine perspective, we were interested

[1]Memory and Aging Center, Department of Neurology, Weill Institute for Neurosciences, University of California, San Francisco, San Francisco, CA, USA. [2]Molecular Biophysics and Integrated Bioimaging Division, Lawrence Berkeley National Laboratory, Berkeley, CA, USA. [3]Helen Wills Neuroscience Institute, University of California, Berkeley, Berkeley, CA, USA. [4]Department of Radiology and Biomedical Imaging, University of California, San Francisco, San Francisco, CA, USA.
*Corresponding author. Email: renaud.lajoie@ucsf.edu

in testing PET imaging's ability to predict neuroimaging changes at the individual patient level. On the basis of the cross-sectional evidence described above, we hypothesized that higher baseline FTP-PET, but not PIB-PET, would be associated with higher atrophy rates and that the topography of FTP-PET binding would predict the pattern of subsequent atrophy at the individual patient level. We had two secondary aims. First, we tested whether baseline PIB and FTP-PET data could help predict patients' clinical deterioration, measured with the clinical dementia rating scale sum of boxes (CDR-SB), a measure of disease severity based on functional decline (*20*). Last, we investigated whether the previously highlighted association between earlier age of onset and greater atrophy rates could be explained by baseline differences in tau burden.

Table 1. Patients included in the analyses. For continuous variables, mean ± SD [min, max] is indicated. MMSE, mini-mental state examination; CDR-SB, clinical dementia rating scale sum of boxes.

Sex: n_{female}/n_{male}	21/11
Age at baseline	64 ± 9 [49, 83]
Education	17 ± 3 [12, 24]
APOE4 alleles: $n_0/n_1/n_2$ ($n_{missing}$)	14/13/3 (2)
MMSE at baseline	24 ± 4 [14, 30]
CDR-SB at baseline	3.8 ± 2 [0, 8]
Baseline to follow-up MRI (months)	15 ± 3 [10, 24]
Baseline MRI to FTP-PET (months)	1.8 ± 2.2 [0, 7.7]
Baseline MRI to PIB-PET (months)	1.6 ± 2.3 [0, 7.7]

RESULTS

Description of the cohort

The current study included 32 patients in early clinical stages of AD (mild cognitive impairment or mild dementia, and a positive PIB-PET scan). All patients underwent structural MRI and PET with both PIB and FTP at the baseline visit, and a second structural MRI at a follow-up visit (median time interval, 15 months). Two Siemens 3-T MRI scanners were used in this study (see Materials and Methods and Discussion). Demographics are presented in Table 1. The sample was heterogeneous and included six patients fulfilling criteria for logopenic variant primary progressive aphasia (*21*) and three patients meeting criteria for posterior cortical atrophy (*22*)). Patients were between 49 and 83 years old at the time of PET scan [20 patients (63%) being under 65 years old].

At the group level, longitudinal atrophy is greater in regions with high baseline FTP binding

For each patient, baseline PET scans were processed to calculate standardized uptake value ratio (SUVR) maps [see (*23*) and Materials

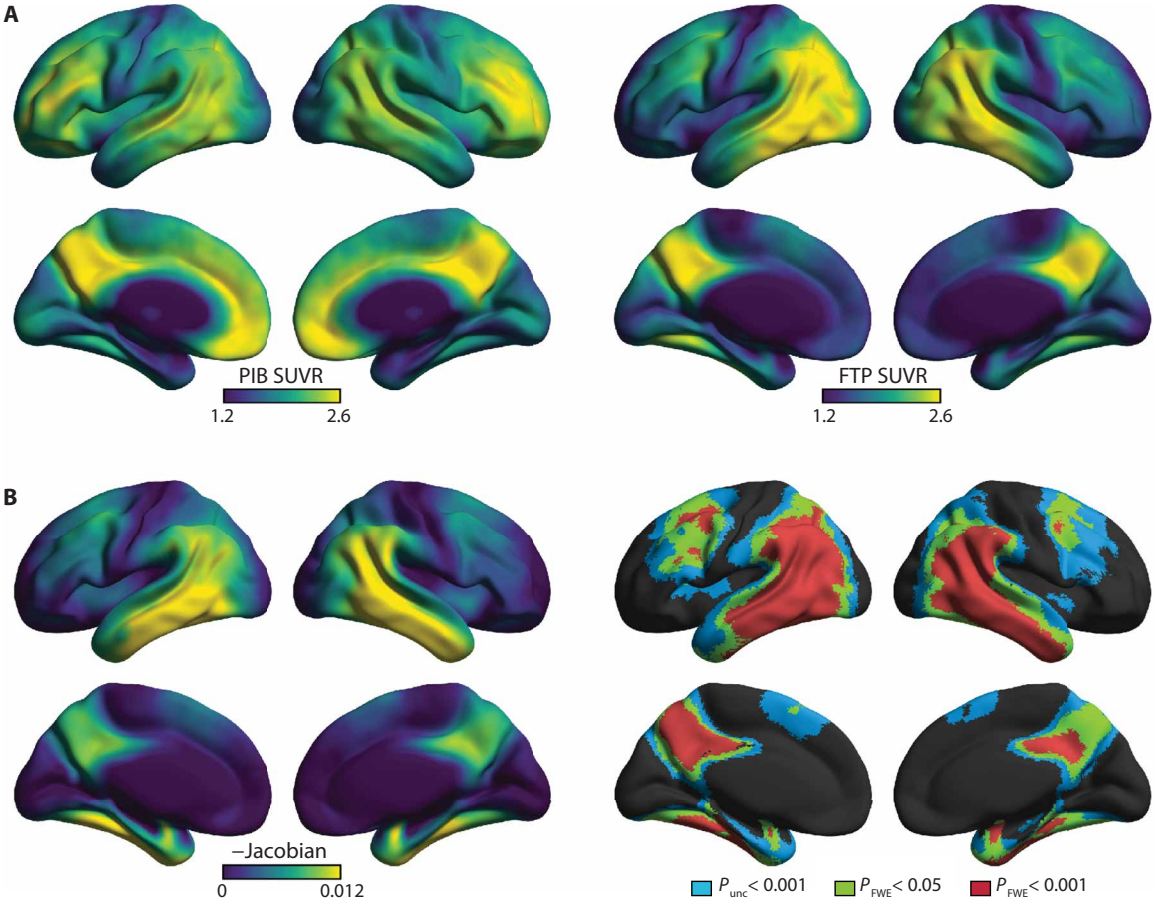

Fig. 1. Voxelwise patterns at the group level. (**A**) Group-average PET SUVR maps at baseline. (**B**) Voxelwise pattern of longitudinal cortical atrophy. Left: Average of 32 reversed GM-masked and smoothed reversed Jacobian maps (higher value means higher rate of atrophy). Right: Statistical map corresponding to a voxelwise one-sample *t* test including the 32 individual maps, showing areas of significant atrophy (reversed Jacobians > 0) based on three increasingly conservative thresholds [$P_{uncorrected}$ < 0.001, family-wise error (FWE)–corrected P_{FWE} < 0.05 and P_{FWE} < 0.001 at the voxel level; all three with P_{FWE} < 0.05 at the cluster level]. All maps are available for visualization at https://neurovault.org/collections/WLDODMCY/.

and Methods for more details]. The two MRI scans were processed using a specific longitudinal pipeline (*24*) to derive a three-dimensional (3D) map of Jacobians representing annualized atrophy (Jacobians were reversed so that positive values indicate tissue shrinkage over time). All maps were masked to restrict the investigations to the cortical gray matter (GM) (fig. S1) and analyzed in native or template space, depending on the analysis. We first created group-average images of PIB, FTP, and longitudinal atrophy using images warped to template space (Fig. 1).

PIB binding predominated in medial areas (prefrontal and posterior cingulate/precuneus regions); signal was also elevated in lateral frontal and temporo-parietal cortices (Fig. 1A). FTP binding was maximal at the temporo-parietal junction and the posterior cingulate/precuneus and moderate in dorsal frontal, occipital, and infero-medial temporal cortices (Fig. 1A).

The pattern of longitudinal atrophy is shown in Fig. 1B as the group-average reversed Jacobian map (higher values indicating higher atrophy rates) and as a statistical map based on a one-sample *t* test performed on the 32 Jacobian maps. Atrophy was maximal in temporo-parietal areas, posterior cingulate/precuneus, and dorsal frontal areas, surviving stringent family-wise error (FWE) correction ($P_{FWE} < 0.001$) in those regions where baseline FTP-PET signal was particularly elevated.

Patients with high baseline FTP-PET binding develop more severe cortical atrophy

We investigated the relationships between baseline cortical alterations (PIB SUVR, FTP SUVR, and cortical thickness) and the severity of subsequent atrophy across patients. Figure 2 shows the associations between baseline global (mean of entire cortex) measures of PIB-SUVR, FTP-SUVR, and cortical thickness [values were derived from FreeSurfer 5.3, *Z*-scored based on normative dataset (*25*), and reversed so higher values indicate lower baseline thickness] and overall cortical atrophy (average reversed cortical Jacobian values). Longitudinal cortical atrophy was strongly associated with baseline FTP {$r_{FTP\text{-}atrophy}$ = 0.670, 95% confidence interval (CI) [0.388, 0.841], $P < 0.001$}, in contrast with weaker correlations with baseline cortical PIB ($r_{PIB\text{-}atrophy}$ = 0.291, 95% CI [−0.029, 0.546], $P = 0.07$) and baseline global cortical thickness ($r_{thickness\text{-}atrophy}$ = 0.281, 95% CI [−0.067, 0.586], $P = 0.12$). Pairwise comparisons of correlations (based on bootstrapping of correlation coefficient pairs with 5000 permutations) showed that longitudinal atrophy was more strongly correlated with FTP than PIB ($\Delta r = 0.379$, 95% CI [0.121, 0.594], $P = 0.004$), but the difference between $r_{FTP\text{-}atrophy}$ and $r_{thickness\text{-}atrophy}$ was not significant at $\alpha = 0.05$ ($\Delta r = 0.390$, 95% CI [−0.119, 0.821], $P = 0.11$).

When including all three baseline predictors in a single multiple regression model to predict subsequent longitudinal atrophy, FTP remained significant (standardized $\beta = 0.696$, $t = 4.2$, $P < 0.001$ versus $\beta = -0.083$, $t = -0.5$, $P = 0.58$ for PIB and $\beta = 0.173$, $t = 1.3$, $P = 0.22$ for thickness; see table S1), and this full model did not perform better than a model including FTP only to predict longitudinal atrophy (table S1).

Voxelwise FTP-PET patterns predict maps of subsequent atrophy at the individual patient level

We next assessed whether the topography of PIB and FTP binding could help predict the pattern of atrophy at the individual patient level, using a voxelwise approach. For each patient, the topographical similarity between 3D maps of PET binding and atrophy was quantified using a voxelwise spatial correlation approach restricted to a cortical mask, as previously described (*26*) and illustrated in Fig. 3A (see fig. S1 for details on the preprocessing). Resulting spatial correlation coefficients (baseline PIB to longitudinal atrophy and baseline FTP to longitudinal atrophy) were then *z*-transformed to allow analysis at the group level (see Fig. 3B). Across the 32 patients, spatial correlation between baseline PIB and subsequent atrophy was minimal: mean $z(r) = 0.183$, 95% CI [0.131, 0.226] (percentile bootstrap CI based on 5000 permutations), indicating 3% [2%, 5%] shared variance on average. In contrast, the spatial correlation between baseline FTP and longitudinal atrophy was high: mean $z(r) = 0.780$, 95% CI [0.682, 0.859], indicating 43% [35%, 48%] shared variance on average. Spatial correlation with longitudinal atrophy was significantly higher for baseline FTP than PIB [paired *t* test conducted on the $z(r)$ values: $t(31) = 14.9$, $P < 0.001$]. Note that correlations were higher for FTP than for PIB in all 32 patients, as shown in Fig. 3B.

Baseline tau-PET predicts longitudinal atrophy independent of baseline thickness

Our finding that baseline FTP-SUVR correlates with subsequent atrophy could be confounded by the fact that these regions are usually

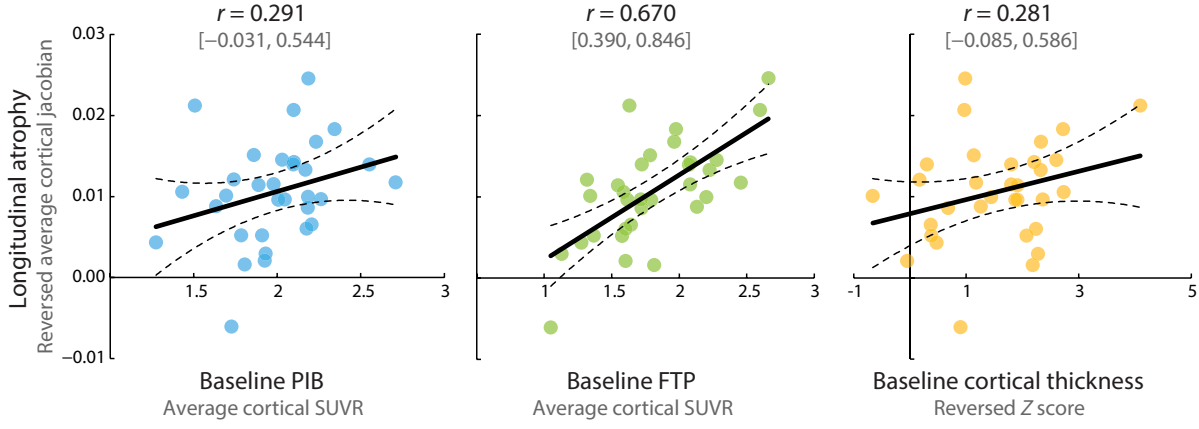

Fig. 2. Bivariate associations between baseline measures and subsequent atrophy across the 32 patients. Ninety-five percent confidence intervals (95% CI) were computed using bootstrapping with 5000 permutations. Details about the statistical analyses, including a multiple regression with all three baseline predictors, are available in Results and table S1.

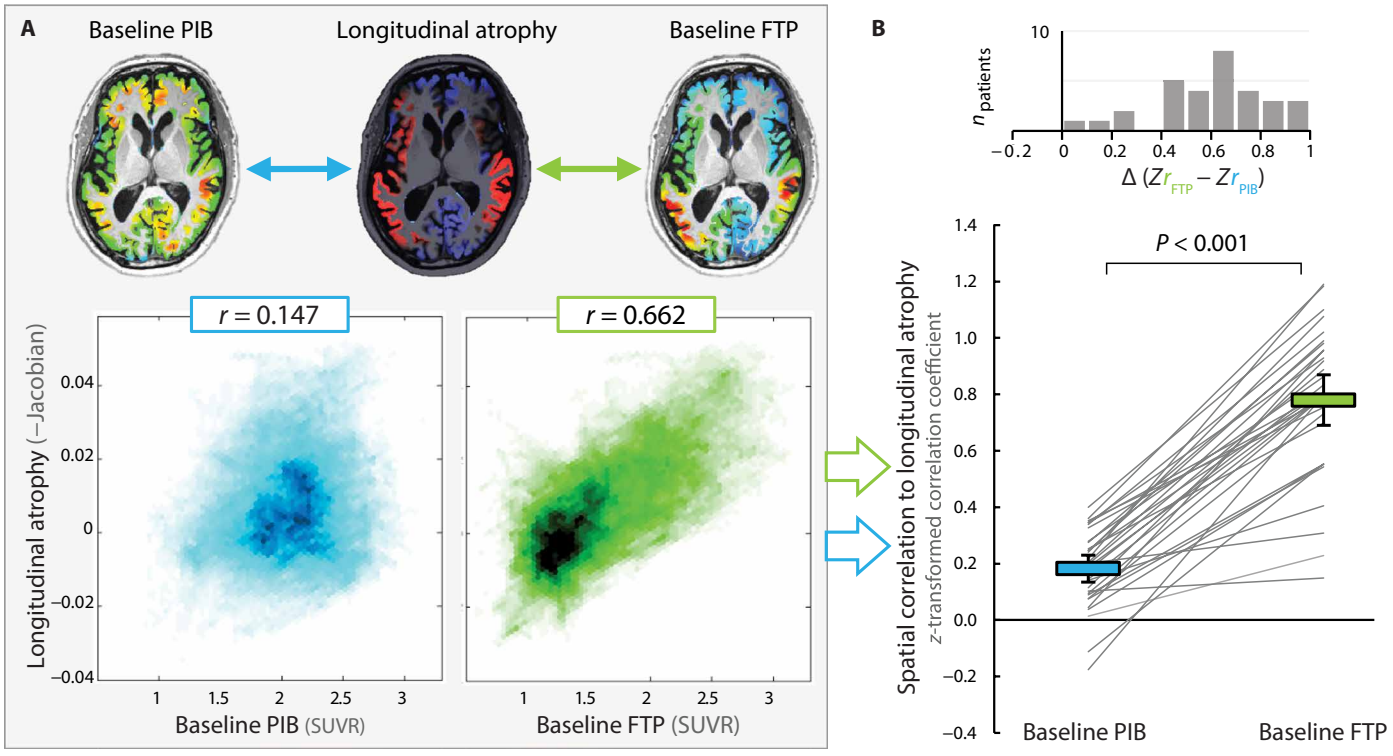

Fig. 3. Voxelwise spatial correlations between baseline PET patterns and the topography of subsequent atrophy. (**A**) Analyses conducted at the individual patient level to quantify the similarity between patterns of PET SUVR at baseline and maps of longitudinal atrophy (reversed Jacobians). The images used for illustration correspond to a patient with close-to-average values. For each patient, correlations were assessed on all voxels of the cortex (see fig. S1 for details about specific image preprocessing steps). (**B**) Group-level analyses. Resulting correlation coefficients were *z*-transformed to be analyzed at the group level. Gray lines show individual patients, whereas colored bars indicate average *z*-transformed coefficients (with 95% CI). *P* value corresponds to two-tailed paired *t* test. The top panel shows the histogram of the difference between *z*-transformed spatial correlation coefficients between PIB and atrophy and FTP and atrophy across all 32 patients, highlighting that the latter was higher than the former in all 32 cases.

already atrophic at baseline and that atrophy tends to accelerate locally. In addition, low cortical thickness at baseline could reduce the PET signal due to partial volume effects and introduce additional noise in the measurements. We therefore conducted additional analyses to assess the potential confounding effect of "baseline atrophy" on the association between FTP-PET and subsequent atrophy at a regional level. This set of analyses was conducted using regions of interests, enabling the use of partial volume corrected (PVC) PET data. Each patient's cortex was segmented into 68 regions of interest (ROIs) using FreeSurfer 5.3, and the average cortical thickness was extracted from the baseline MRI for each ROI. For each patient, cortical thickness values were converted to a *Z* score (based on normative data, see Materials and Methods) to be used as indicators of baseline neurodegeneration. Average baseline FTP-SUVR$_{PVC}$ and Jacobian values were also extracted from each ROI (see fig. S2 for details on the preprocessing and Fig. 4A to visualize group averages).

The spaghetti plots in Fig. 4B show that, for most patients, regions with higher baseline FTP-SUVR$_{PVC}$ and, to a smaller extent, lower baseline cortical thickness had higher atrophy rates. Linear mixed-effect models (LMEMs) were used to test the respective contribution of each baseline measure to longitudinal atrophy. All ROIs from all patients were included in LMEMs (68 × 32 = 2176 entries), with random slopes and intercepts for both ROI and patient factors (see table S2 for further details on model specifications and results). Separate LMEMs were first conducted for each predictor, and both were significant ($P < 0.001$; see Fig. 4B, bottom right panel), although FTP$_{PVC}$ was a stronger predictor ($t = 12.6$, marginal $R^2 = 0.444$, conditional $R^2 = 0.785$) than baseline thickness ($t = 5.1$, marginal $R^2 = 0.057$, conditional $R^2 = 0.610$). However, when entering both predictors in the same model (Fig. 4B, bottom line), only FTP$_{PVC}$ was significant ($t = 11.9$, $P < 0.001$ versus $t = -1.7$, $P = 0.09$ for thickness). In addition, this full model roughly explained the same amount of variance (marginal $R^2 = 0.426$, conditional $R^2 = 0.800$) as the model including baseline FTP$_{PVC}$ only and had a slightly decreased Akaike information criterion (AIC) value (−15,579 versus −15,498; see table S2), indicating that adding baseline thickness only minimally improved the overall model fit. The conclusions of the LMEMs were very similar when using non-PVC PET data and when including baseline PIB-SUVR in the model (see fig. S3).

Baseline tau-PET is more strongly associated with follow-up than baseline cortical thickness

We hypothesized that baseline tau PET will correlate more strongly with cortical thickness measured at follow-up than at baseline, consistent with a conceptual model in which tau deposition precedes neurodegeneration. Figure 5A shows that, at the group level, baseline tau burden (global cortical FTP-SUVR$_{PVC}$) correlated more strongly with global cortical thinning (reversed *Z*-scored thickness) measured at follow-up than baseline ($r = 0.431$, 95% CI [0.166,

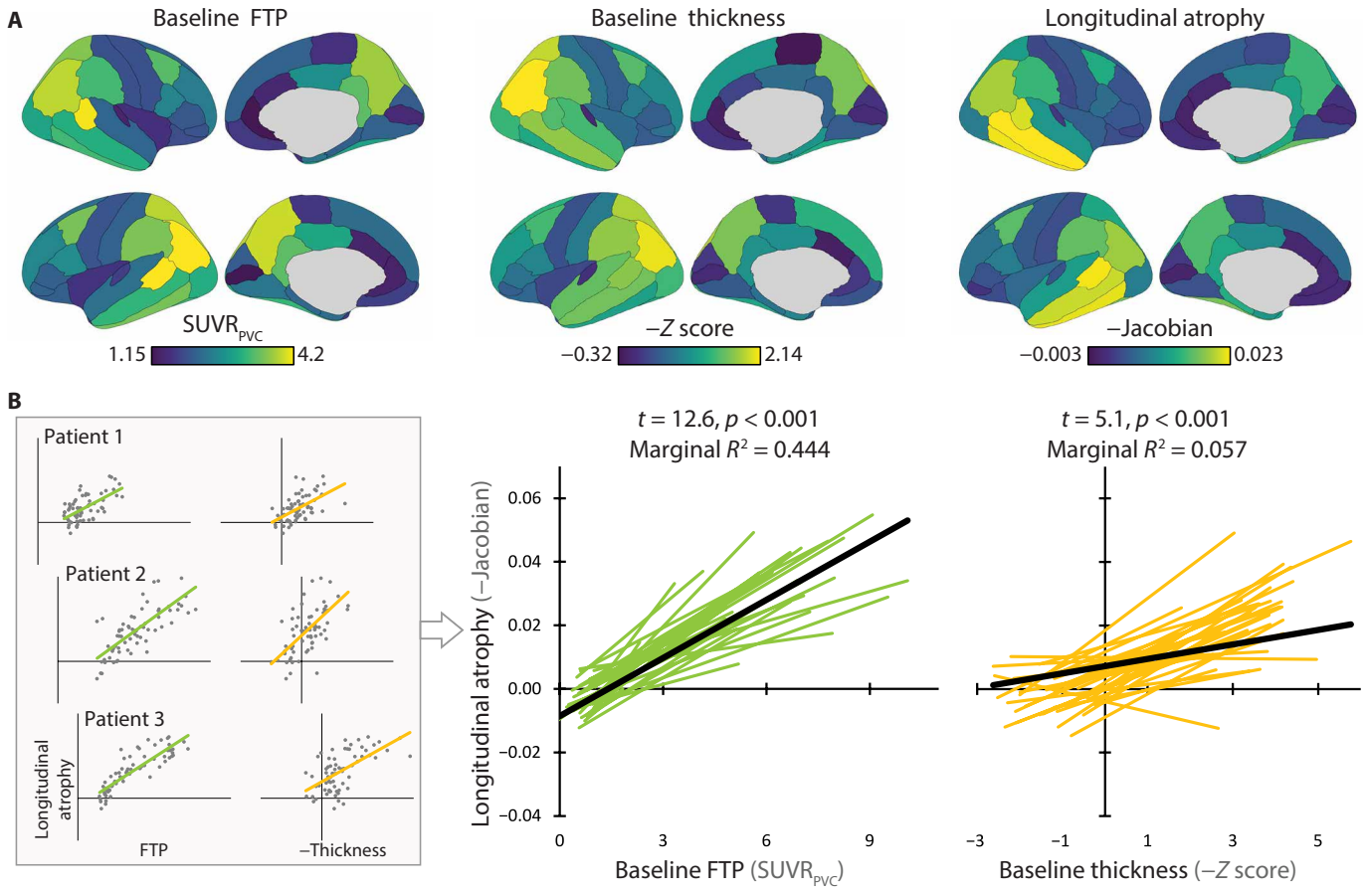

Fig. 4. Relative contribution of baseline partial volume corrected FTP-PET and baseline thickness patterns to predict the topography of subsequent atrophy using FreeSurfer-defined cortical regions of interest. (**A**) Group average values in the 68 FreeSurfer cortical regions of interest (ROIs). The color scale was adapted to the range of values of each modality to best illustrate regional variations. $SUVR_{PVC}$, partial volume corrected standardized uptake value ratio. (**B**) Spatial associations between patterns of baseline FTP-$SUVR_{PVC}$, thickness, and longitudinal atrophy were conducted for each patient on the basis of the 68 ROIs, as illustrated in the left panel. The spaghetti plots on the right illustrate the 32 regression lines obtained at the patient level for each pair of variables. The statistical indices on top of each spaghetti plot indicate the results of linear mixed-effect models (LMEMs) to predict reverse Jacobians; separate models were run with each of the two baseline variables as a predictor. A full model that included both predictors together is described in Results and table S2.

0.663] versus r = 0.168, 95% CI [−0.150, 0.480], Δr = 0.263, bootstrapped 95% CI [0.026, 0.517], P = 0.026).

We also tested the spatial similarity between baseline tau-PET and cortical thinning measured at each time point (Fig. 5B). The method was similar to that presented in Fig. 3, except that the patient-level analysis was conducted using ROIs rather than voxelwise, enabling the calculation of Z score thickness values as mentioned above (see fig. S2). Across the 32 patients, baseline FTP_{PVC} spatially correlated with concurrent cortical thickness: mean spatial correlation $z(r)$ = 0.787, 95% CI [0.681, 0.876], indicating 43% [35%, 50%] shared variance on average. Yet, the spatial correlation was higher between baseline FTP_{PVC} and follow-up thickness patterns: mean $z(r)$ = 0.833, 95% CI [0.727, 0.921], indicating 47% [39%, 53%]; paired t test on the $z(r)$ values: $t(31)$ = 2.86, P = 0.008.

Longitudinal precuneus atrophy parallels clinical decline

The CDR-SB was used to measure clinical progression; to control for variations in clinical follow-up duration (mean = 15.0 months, min = 11.1, max = 23.7), changes in CDR-SB were annualized [(follow-up − baseline)/time interval]. On average, CDR-SB increased by 1.6 ± 2.0 points per year [one-sample t test: $t(31)$ = 4.52, P < 0.001].

Annualized CDR-SB increase was poorly correlated with global cortical measures of baseline PIB SUVR (r = −0.125, P = 0.51), FTP SUVR (r = −0.041, P = 0.80), cortical thickness (r = 0.006, P = 0.95), or longitudinal atrophy (r = 0.095, P = 0.65; see fig. S4 for 95% CI and scatter plots). Voxelwise analyses showed that increase in CDR-SB over time was associated with longitudinal atrophy in the precuneus/posterior cingulate area (surviving FWE correction at the voxel level; see fig. S4). In contrast, no regional association was found in any of the three baseline predictors (based on the $P_{uncorrected}$ < 0.001 threshold).

Earlier disease onset is associated with higher tau burden and thus more rapid atrophy

Older age at baseline was associated with lower baseline abnormalities (fig. S5), although the correlation only reached statistical significance (at α = 0.05) for baseline FTP-SUVR (r = −0.572, P = 0.002), but not baseline PIB-SUVR (r = −0.313, P = 0.07) and baseline thickness (r = −0.224, P = 0.12; see Fig. 6A for 95% CI and scatter plots). In addition, older patients had lower rates of atrophy (correlation between age and reversed average cortical Jacobian: r = −0.542, P = 0.006; Fig. 6A). When including both patient's age

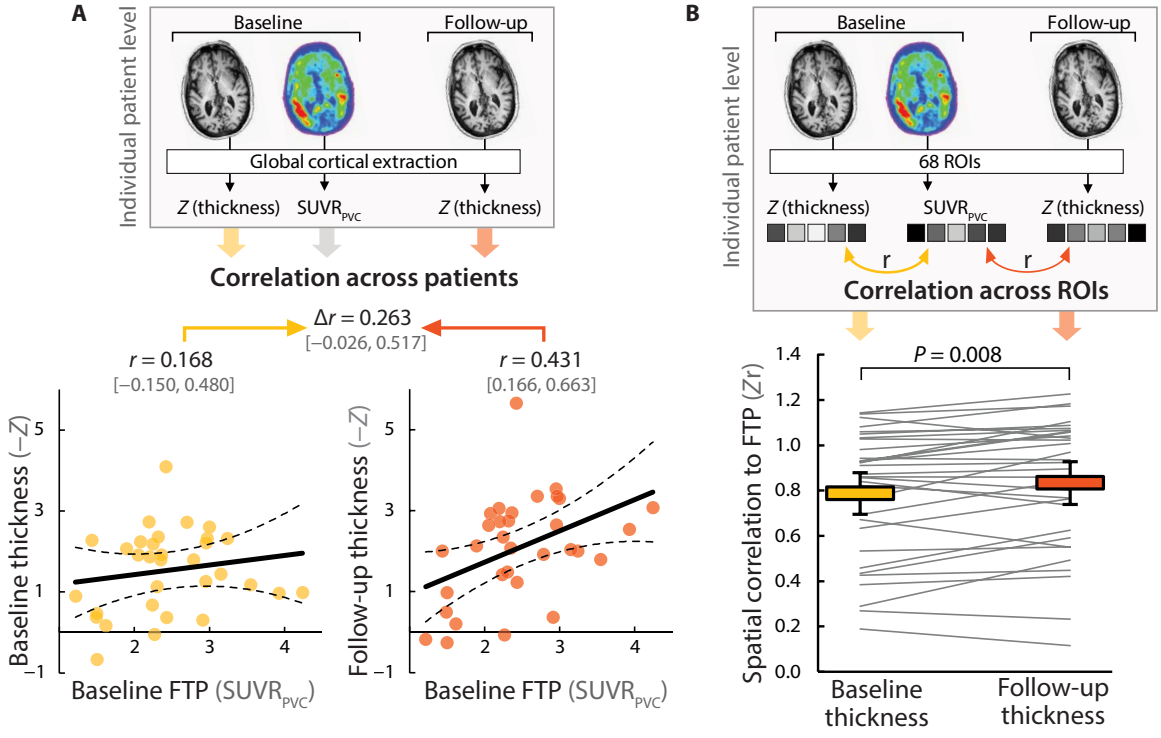

Fig. 5. Association between baseline FTP-PET and cortical thickness at baseline and follow-up. (**A**) Association between baseline global cortical PVC FTP-SUVR values and cortical thickness at baseline (yellow) and follow-up (orange) across patients. Cortical thickness measures were *Z*-scored on the basis of normative data and reversed, so higher values indicate more neurodegeneration. Ninety-five percent CIs are based on bootstrap with 5000 permutations. (**B**) Spatial similarity between FTP-SUVR$_{PVC}$ and low cortical thickness at each time point was assessed at the single patient level using a correlation approach based on FreeSurfer ROIs (top panel). Cortical thickness was extracted from 68 FreeSurfer cortical ROIs, transformed into a Z score using normative data, and reversed to higher values to indicate more neurodegeneration; FTP-SUVR$_{PVC}$ values were extracted from each ROI. Correlations were Fisher *z*-transformed to be analyzed at the group level (bottom panel). Each gray line represents a single patient, and color bars illustrate group averages with bootstrap 95% CIs. *P* value corresponds to a paired *t* test, showing that patterns of baseline FTP binding are more similar to patterns of low cortical thickness at follow-up than baseline.

and baseline cortical FTP-SUVR in a multiple regression model, FTP remained highly predictive of longitudinal atrophy (standardized β = 0.536, $P = 0.003$), while the effect of age was reduced (standardized β = −0.235, $P = 0.16$). Mediation analyses further showed that the relationship between patient's age and longitudinal rate of atrophy was at least partly mediated by baseline cortical FTP-SUVR (Fig. 6A). No mediation effect was found using baseline PIB-SUVR or baseline cortical thickness (see fig. S6). Voxelwise analyses showed that both FTP-SUVR and longitudinal atrophy decreased with greater patient age throughout the brain (Fig. 6B) and most strongly in the fronto-parietal areas where correlations reached statistical significance ($P_{unc} < 0.001$ at the voxel level with $P_{FWE} < 0.05$ at the cluster level; see fig. S7).

Last, the spatial similarity between baseline FTP-SUVR maps and patterns of subsequent atrophy (quantified at the individual patient level using the voxelwise spatial correlation method described in Fig. 3) decreased with age ($r = -0.471$, $P = 0.005$) (see Fig. 6B). Spatial correlation values went from an estimated $z(r) \sim 0.9$ at age 55 (R^2 = 52% shared variance) to $z(r) \sim 0.63$ at age 75 (R^2 = 31% shared variance). The spatial correlation between baseline PIB and longitudinal atrophy was low regardless of patient's age ($r = -0.253$, $P = 0.13$; see fig. S5 for 95% CI and scatter plots).

DISCUSSION

In this prospective longitudinal neuroimaging study conducted in patients at early clinical stages of AD, we investigated the associations between baseline PET measures of tau and Aβ burden and subsequent neurodegeneration measured as MRI atrophy over time. In line with our original hypotheses, we found that baseline tau PET, but not Aβ-PET, predicted the degree and spatial distribution of cortical atrophy over the subsequent year.

The association between baseline FTP-PET and subsequent atrophy, and notably the topographical similarity between the two patterns, was a strong and robust finding. The association was found at both the group (Figs. 1 and 2) and the individual patient levels (Figs. 3 and 4) and using complementary voxelwise (Fig. 3) and ROI-based (Fig. 4 and 5 and fig. S3) approaches. The predictive value of the baseline tau-PET pattern on future atrophy remained substantial even after adjusting for baseline cortical thickness, with tau-PET explaining ~40% of unique variance in longitudinal atrophy. Last, although cross-sectional relationships can be found between tau-PET and concurrent neurodegeneration, we showed that tau-PET more closely resembles neurodegeneration at a future time point (Fig. 5). Together, these longitudinal results expand on previous findings from postmortem and cross-sectional studies, by providing prospective evidence that the aggregation of tau predicts future neurodegeneration in patients with biomarker-confirmed AD. These results support a sequential relationship between tau fibrillar aggregates and downstream degeneration. This directionality is in line with a recent longitudinal tau-PET study from our group showing that, at the clinical stage of AD, tau pathology and brain atrophy progress in different regions, likely reflecting a phase shifting, with tau elevation locally preceding atrophy (*27*).

Multiple studies (*28*–*31*) previously reported that baseline cerebrospinal fluid (CSF) concentration of tau was associated with

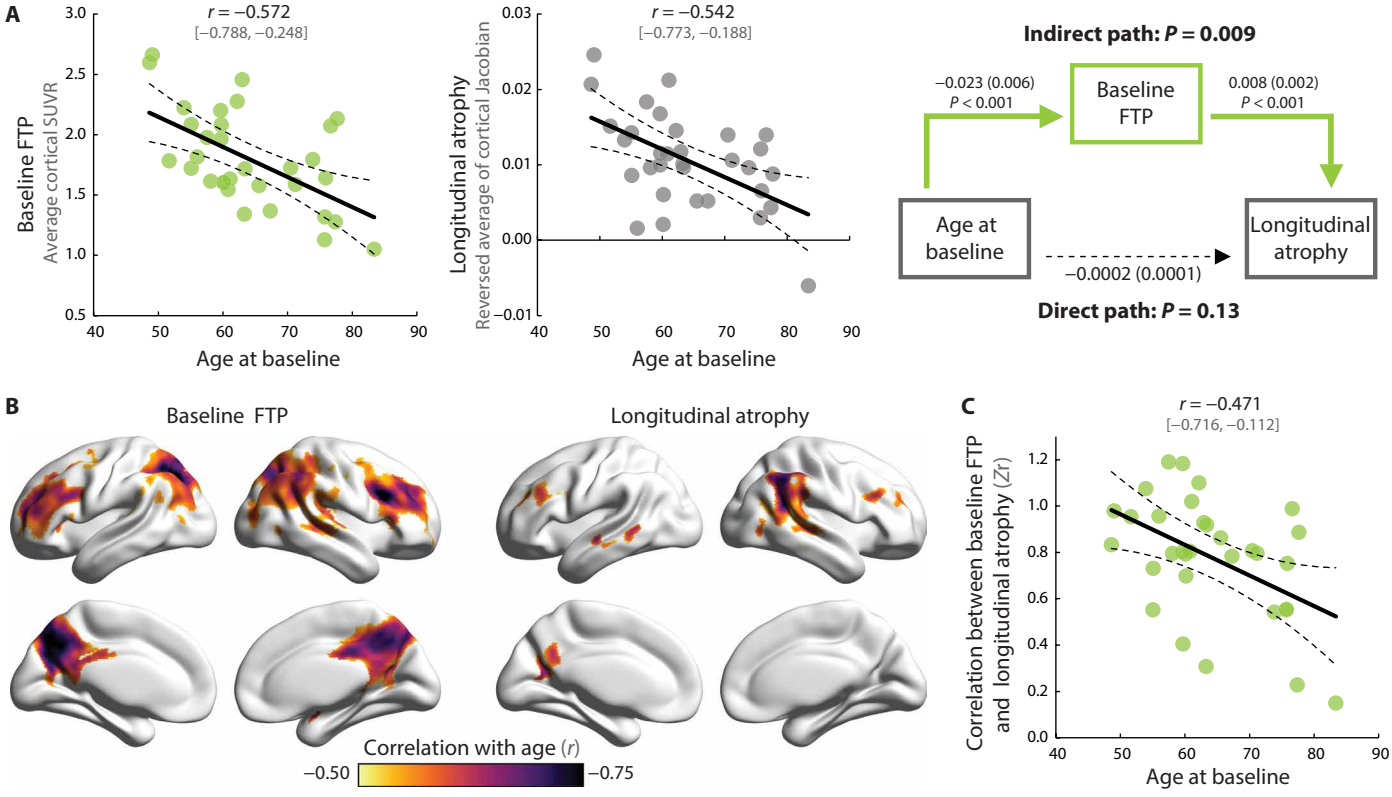

Fig. 6. Effect of patient age on baseline tau pathology and subsequent atrophy. (**A**) Association between patient age and global cortical FTP-SUVR at baseline and longitudinal atrophy; see fig. S5 for associations between age and other variables. Mediation analysis showed that baseline cortical FTP-SUVR mediated the effect of age on longitudinal atrophy; see fig. S6 for the (nonsignificant) mediation models conducted with baseline PIB and baseline thickness instead of baseline FTP. (**B**) Voxelwise analyses showing the regional associations between increasing patient's age and lower FTP-SUVR or atrophy rates (see fig. S7 for unthresholded maps and https://neurovault.org/collections/WLDODMCY/ to access the 3D maps). (**C**) Association between patient's age and the topographical similarity between patterns of baseline FTP-SUVR and subsequent atrophy measured using voxelwise spatial correlation (as described in Fig. 3); see fig. S5 for similar plot with PIB.

higher atrophy rates in heterogeneous groups of patients, although contradicting results exist (*32*, *33*). Our finding of an association between global cortical FTP and global cortical atrophy (Fig. 2A) confirms that this relationship is not driven by the inclusion of AD (high biomarker, high atrophy) and controls or non-AD (low biomarker, low atrophy) patients, but exists within a group of patients with biomarker-confirmed AD. The replicability of the tau biomarker/subsequent atrophy association across biomarker types (fluid versus imaging) is also consistent with the relationships found between PET and CSF measures of tau (*23*, *34*, *35*). The topographical information embedded in the PET data constitutes a major advantage compared to CSF markers. We demonstrated that tau-PET is not only predictive of how much but also of where atrophy will occur, which has major implications for patient prognosis and clinical trials.

Our findings suggest that tau-PET could be useful for the design of clinical trials and could increase the ability to detect a treatment effect even over a relatively short time frame (*36*, *37*). First, tau-PET could be used to enrich trials with patients with tau-PET signal predictive of upcoming atrophy or to stratify patients in trials based on the degree of expected atrophy in the upcoming year. Second, tau-PET could help determine how (i.e., where) atrophy should be measured to maximize study sensitivity. A major issue of using MRI to monitor disease progression is the interindividual heterogeneity in atrophy patterns (*38*), even when selecting patients with a classic amnestic phenotype as in the Alzheimer's Disease Neuroimaging Initiative (*12*, *39*). A given generic ROI (e.g., the hippocampus) would not optimally capture every patient's brain atrophy [e.g., patients with "hippocampal-sparing AD" (*38*, *40*)]. Alternative options exist to maximize detection of AD atrophy using data-driven ROIs (*41*) or adapting the ROI to specific phenotypes (*42*), but our data suggest that PET could be used to create patient-tailored, FTP-informed ROIs for atrophy detection. This approach could capture tau-mediated neurodegeneration in every patient in a more optimal manner, agnostic of any a priori assumptions. Alternatively, the tight relationship between tau and atrophy might imply that, in regions with elevated tau-PET signal, the pathological cascade leading to neurodegeneration has already been triggered and that neurodegeneration processes are now uncoupled from tau pathology. In that case, anti-tau therapies could be more effective in preventing atrophy in regions with low to mild tau-PET signal, whereas atrophy in high tau-PET regions would be difficult to modify with anti-tau therapies.

Clinical decline measured with the CDR-SB was associated with atrophy in the precuneus but was not correlated with baseline FTP-PET. This weak relationship might be related to methodological factors: the small sample size, the intrinsic noise of measuring clinical progression based on two time points, or the use of memory-centric

CDR-SB in a clinically diverse cohort like ours that includes language, and visuospatial-predominant AD phenotypes. Alternatively, the lack of correlation with FTP could also reflect the indirect relationship between tau pathology and clinical deficits that is thought to be at least partly mediated by brain degeneration (*10*).

In contrast to tau-PET, neither the burden nor topography of Aβ-PET was a strong predictor of future atrophy. This is consistent with multiple reports that Aβ-PET has no or weak relationships with the patterns of neurodegeneration or clinical deficits at symptomatic stages (*8*, *43*), although associations might be found at earlier (preclinical) stage (*44*). The quantitative and topographical dissociation between Aβ and neurodegeneration is also consistent with autopsy data (*45*, *46*). To our knowledge, the relationships between baseline volume or thickness and future atrophy have not been thoroughly investigated, but studies have suggested that atrophy accelerates over time, before decelerating in later stages (*18*, *19*). This nonlinear relationship might explain why we could not identify consistent and robust relationships between baseline MRI findings and subsequent atrophy.

Baseline tau-PET accounted for ~40 to 50% of the severity and topography of subsequent atrophy in our cohort. Future investigations will be needed to study additional predictors of atrophy [e.g., inflammation (*47*), nonlocal effects of pathology (*48*, *49*), or additional brain pathologies (*50*)] to further our understanding of the complex mechanisms underlying neurodegeneration in AD.

Our analyses identified patient's age as an important factor regarding not only the severity of tau burden and brain atrophy but also the relationship between pathology and longitudinal atrophy. First, we replicated previous findings that later age of disease onset is associated with lower tau-PET burden (*8*, *11*) and longitudinal atrophy rates (*12*–*14*). Moreover, we showed that the spatial association between FTP and longitudinal atrophy sharply decreased with patient's age (Fig. 5), in line with a recent cross-sectional study (*51*). Together, these results are consistent with the idea that early-onset AD might constitute a more pure form of AD in which neurodegeneration is mainly driven by AD pathology, whereas later-onset clinical AD is multifactorial, associated with distinctive risk factors, and related to more frequent co-morbidities and co-pathologies (*52*, *53*). Previous clinicopathological studies showed that the relationship between AD neuropathology and dementia decreased in older patients (*54*). Together, growing evidence suggests that potential disease-modifying drugs that specifically target AD neuropathology may benefit patients with earlier-onset AD more than older patients.

A number of study features and limitations should be highlighted to appropriately interpret our results. First, note that PET signal is only a proxy for underlying pathology, and although postmortem studies suggest that FTP binds to paired helical filaments of tau (*55*, *56*), "off target" signal unrelated to tau in the basal ganglia (*57*, *58*) and in some tau-negative conditions (*59*, *60*) raises questions about specificity. Second, the sample size was modest, though similar to previous cross-sectional tau-PET/atrophy association studies. The use of complementary robust statistical approaches, and the inspection of all scatter plots and images, showed that results were not influenced by outliers. Third, the patients included in our study constitute an academic-based cohort of diverse and relatively young patients, which may limit generalizability. Note that the results remained unchanged when excluding non-amnestic variants (language or visuospatial phenotypes of AD; see fig. S8). Fourth, our cohort encompassed early clinical stages of AD, and the results cannot be extrapolated to earlier (i.e., preclinical) or more severe stages of the disease, when neurodegeneration might be associated or driven by distinct mechanisms. Fifth, because of the recent development of FTP, patients only had one follow-up MRI after the baseline visit, and additional time points would enable a more precise characterization of atrophy trajectories. Future studies will be needed to determine the prognostic value of baseline tau-PET over longer follow-up. Similarly, clinical decline was evaluated on the basis of two time points only, and more data would be needed to improve signal to noise; the limited available time points, together with the heterogeneity of the cohort, might account for the lack of associations between baseline tau-PET and clinical decline. Last, our patients underwent MRI scanning on two different Siemens 3-T scanners, which might have added noise to the estimation of longitudinal atrophy. However, further analyses showed that the present results were found independently of MRI scanning protocol (fig. S9).

In summary, our study illustrates the potential of PET imaging to identify the pathological drivers of neurodegeneration in AD and to help predict individual patients' future evolution. These results outline the robust local relationships between accumulation of tau-containing paired helical filament and neurodegeneration, emphasizing tau as a relevant target for disease-modifying drugs at this early clinical stage (*61*). Additional studies will be needed to extend our approach to larger cohorts, notably considering additional disease stages, older age of onset, and longer follow-up duration.

MATERIALS AND METHODS

Experimental design

The main objective of this study was to test whether amyloid and tau-PET could predict future brain atrophy in patients at symptomatic stages of AD. Data were derived from an ongoing longitudinal observational study including repeated MRI, PIB-PET, and FTP-PET in patients with a clinical diagnosis of AD at the mild cognitive impairment or dementia stage. No power analysis was performed before the study, but the sample size is within the range of previous papers assessing relationships between tau-PET and brain volume in symptomatic patients (*6*–*7*, *17*). Data preprocessing steps were performed using automated pipeline agnostic of the baseline tau- and amyloid-PET data. Quality control of the preprocessing steps was done blind to the baseline PET measures. No outlier was detected, and all data were included in all analyses and plotted on each figure.

Patients

All patients underwent a comprehensive clinical evaluation (*10*) at the University of California, San Francisco (UCSF) Memory and Aging Center. We selected patients who (i) had a clinical diagnosis of AD [at either the mild cognitive impairment or dementia stage (*62*, *63*)], (ii) had undergone 3-T structural MRI, FTP-PET, and PIB-PET at their baseline visit, (iii) had a positive PIB-PET [based on visual read (*64*)], and (iv) had a follow-up 3-T MRI at least 9 months after the first visit. By 1 December 2018, 36 patients fulfilled these criteria, but 4 were excluded because of movement artifacts on an MRI and/or failure of the longitudinal MRI pipeline. The remaining 32 patients were included in the analyses.

Written informed consent was obtained from all patients or their surrogates. The study was approved by the University of California (San Francisco and Berkeley) and Lawrence Berkeley National Laboratory institutional review boards for human research.

Image acquisition

T1-weighted magnetization-prepared rapid gradient echo MRI sequences were acquired at UCSF, on either a 3-T Siemens Tim Trio or a 3-T Siemens Prisma Fit scanner. Both scanners had very similar acquisition parameters (sagittal slice orientation; slice thickness, 1.0 mm; slices per slab, 160; in-plane resolution, 1.0 × 1.0 mm; matrix, 240 × 256; repetition time, 2300 ms; inversion time, 900 ms; flip angle, 9°), although echo time slightly differed (Trio, 2.98 ms; Prisma, 2.9 ms).

PET data were acquired on a Siemens Biograph PET/computer tomography (CT) scanner at the Lawrence Berkeley National Laboratory. Both radiotracers were synthesized and radiolabeled at the Lawrence Berkeley National Laboratory's Biomedical Isotope Facility. Here, we analyzed PET data that were acquired from 50 to 70 min after the injection of ~15 mCi of PIB (four 5-min frames) and 80 to 100 min after the injection of ~10 mCi of FTP (four 5-min frames). A low-dose CT scan was performed for attenuation correction before PET acquisition, and PET data were reconstructed using an ordered subset expectation maximization algorithm with weighted attenuation and smoothed with a 4-mm Gaussian kernel with scatter correction (calculated image resolution, 6.5 × 6.5 × 7.25 mm based on Hoffman phantom).

SUVR calculation

Each patient's baseline MRI was segmented using FreeSurfer 5.3 (https://surfer.nmr.mgh.harvard.edu/) and Statistical Parametric Mapping 12 (SPM12; Wellcome Department of Imaging Neuroscience, Institute of Neurology, London, UK) to create tracer-specific PET reference regions. PET frames were realigned, averaged, and coregistered onto their corresponding MRI. SUVR images were created using FreeSurfer-defined cerebellar GM for PIB-PET. For FTP, FreeSurfer segmentation was combined with the SUIT template (*65*) (which was reverse-normalized to each patient individual space using SPM12) to only include inferior cerebellum voxels, therefore avoiding contamination from off-target binding in the dorsal cerebellum (*58*, *66*).

Longitudinal pipeline and voxelwise analyses

For each patient, the baseline and follow-up MRIs were processed using SPM12 pairwise longitudinal registration (*24*), creating a within-patient midpoint average MRI and a 3D Jacobian rate map reflecting an annualized measure of volumetric change. In this original Jacobian map, negative values indicate contraction over time (e.g., classically in the brain), whereas positive values indicate expansion (e.g., in the ventricles). The Jacobian maps were reversed (i.e., multiplied by −1), so higher values in the cortex indicate greater atrophy. PIB and FTP-SUVR images were moved from baseline MRI space to the midpoint average MRI space using SPM12's deformation toolbox, to be aligned with the Jacobian rate map.

The mid-point average MRI was then segmented into GM, white matter, and CSF. The tissue segments were used to derive a binary GM mask, which was later masked to exclude basal ganglia [because of FTP off-target binding (*57*) and relative sparing in AD] and cerebellum (i.e., PET reference region) using the Hammers atlas (*67*), resulting in a binary cerebral cortical mask (see fig. S1 for illustration).

The reversed Jacobian rate map and the PET-SUVR images were finally smoothed within this mask using AFNI 3dBlurInMask command and applying differential kernels (4 mm for PET and 8 mm for Jacobians), so all three images had equivalent final smoothness (fig. S1). These images were used to calculate spatial correlations between patterns of atrophy (Jacobian values) and PET binding (Fig. 3).

PIB, FTP, and Jacobian maps from all patients were warped to Montreal Neurological Institute space using the deformation parameters estimated during the midpoint average MRI segmentation step and averaged to create across patient averages for PIB SUVR, FTP SUVR, and Jacobians (Fig. 1). Template-warped Jacobian maps were entered in a voxelwise one-sample *t* test to detect areas of significant atrophy (reversed Jacobians > 0) over time (Fig. 1). All voxelwise results were presented using an uncorrected voxel threshold of $P < 0.001$ combined with a corrected cluster threshold of $P_{FWE} < 0.05$; voxels that reached more conservative voxel-level thresholds ($P_{FWE} < 0.05$ and $P_{FWE} < 0.001$) were also highlighted.

FreeSurfer segmentation and ROI analyses

To quantify baseline cortical neurodegeneration (i.e., in a cross-sectional design), we used the FreeSurfer segmentation outputs derived from the previous step (see the "SUVR calculation" section) and based on the first MRI. The average thickness measure of each of the 68 cortical ROIs was extracted from each patient's FreeSurfer directory and converted into a *Z* score based on the code and the data provided by Potvin *et al.* (*25*). Briefly, patients' thickness values were converted into *Z* scores denoting the deviation from their expected values, as calculated based on the patient's characteristics (age, sex, estimated total intracranial volume, scanner manufacturer, and magnetic field strength) and a normative multicentric sample of 2713 healthy controls aged 18 to 94 years. This approach was previously used to quantify cortical thickness in AD (*68*).

To assess the correlation between the patterns of baseline GM and subsequent atrophy (i.e., are regions that shrink over time already abnormally small at baseline?), we extracted the average SPM12-generated Jacobian values from each of the 68 FreeSurfer ROIs for each patient. Average FTP-PET SUVR values were extracted from all 68 ROIs using a PVC algorithm based on geometric transfer matrix technique [see (*58*, *66*)]. LMEMs were run including all ROIs from all patients (including random slopes and intercepts for both factors), with longitudinal atrophy (Jacobian values) as the dependent variable, and baseline thickness *Z* score and/or $FTP\text{-}SUVR_{PVC}$ as predictors.

Statistical analyses

All statistical analyses were conducted using MATLAB 2015a (MathWorks Inc., www.mathworks.com/) and the Robust correlation toolbox (*69*) to calculate Pearson correlation estimates and percentile bootstrap CI (from which *P* values were derived). Jamovi (www.jamovi.org) was used to conduct multiple regressions, analyses of variance (ANOVAs), mediation analyses, and LMEMs using dedicated modules. Details about each specific analysis are provided with the description of the analyses in Results or the Supplementary Materials.

Imaging results were displayed on 3D brain surfaces using BrainNet Viewer (*70*) and ggseg (https://lcbc-uio.github.io/ggseg/). Data file S1 contains most of the data used in the analyses presented in the article.

SUPPLEMENTARY MATERIALS

stm.sciencemag.org/cgi/content/full/12/524/eaau5732/DC1

Fig. S1. Image processing pipeline related to the voxelwise spatial correlation analyses presented in Fig. 3.
Fig. S2. Image processing pipeline related to the ROI analyses shown in Figs. 4 and 5.
Fig. S3. LMEMs using FreeSurfer-defined cortical ROIs and non-PVC SUVR data (related to Fig. 4 and table S2).
Fig. S4. Associations between neuroimaging measures and clinical decline.
Fig. S5. Association between patient's age and global neuroimaging measures (related to Fig. 6).
Fig. S6. Summary of bivariate associations and mediation models between global cortical neuroimaging measures at baseline, global cortical longitudinal atrophy, and age (related to Fig. 6).
Fig. S7. Voxelwise associations between patient's age, baseline FTP-PET, and longitudinal atrophy (related to Fig. 6).
Fig. S8. Analyses of the influence of atypical AD phenotypes on the main results.
Fig. S9. Analyses of the influence of MRI scanner switch on the main results.
Table S1. Details of linear regression models presented in Fig. 2.
Table S2. Details of LMEMs shown in Fig. 4.
Data file S1. Data used for the analyses presented in the manuscript.

View/request a protocol for this paper from *Bio-protocol*.

REFERENCES AND NOTES

1. B. T. Hyman, C. H. Phelps, T. G. Beach, E. H. Bigio, N. J. Cairns, M. C. Carrillo, D. W. Dickson, C. Duyckaerts, M. P. Frosch, E. Masliah, S. S. Mirra, P. T. Nelson, J. A. Schneider, D. R. Thal, B. Thies, J. Q. Trojanowski, H. V. Vinters, T. J. Montine, National Institute on Aging–Alzheimer's Association guidelines for the neuropathologic assessment of Alzheimer's disease. *Alzheimers Dement.* **8**, 1–13 (2012).
2. C. Duyckaerts, B. Delatour, M.-C. Potier, Classification and basic pathology of Alzheimer disease. *Acta Neuropathol.* **118**, 5–36 (2009).
3. W. E. Klunk, H. Engler, A. Nordberg, Y. Wang, G. Blomqvist, D. P. Holt, M. Bergström, I. Savitcheva, G.-F. Huang, S. Estrada, B. Ausén, M. L. Debnath, J. Barletta, J. C. Price, J. Sandell, B. J. Lopresti, A. Wall, P. Koivisto, G. Antoni, C. A. Mathis, B. Långström, Imaging brain amyloid in Alzheimer's disease with Pittsburgh Compound-B. *Ann. Neurol.* **55**, 306–319 (2004).
4. D. T. Chien, S. Bahri, A. K. Szardenings, J. C. Walsh, F. Mu, M.-Y. Su, W. R. Shankle, A. Elizarov, H. C. Kolb, Early clinical PET imaging results with the novel PHF-tau radioligand [F-18]-T807. *J. Alzheimers Dis.* **34**, 457–468 (2013).
5. H. Cho, J. Y. Choi, M. S. Hwang, J. H. Lee, Y. J. Kim, H. M. Lee, C. H. Lyoo, Y. H. Ryu, M. S. Lee, Tau PET in Alzheimer disease and mild cognitive impairment. *Neurology* **87**, 375–383 (2016).
6. L. Iaccarino, G. Tammewar, N. Ayakta, S. L. Baker, A. Bejanin, A. L. Boxer, M. L. Gorno-Tempini, M. Janabi, J. H. Kramer, A. Lazaris, S. N. Lockhart, B. L. Miller, Z. A. Miller, J. P. O'Neil, R. Ossenkoppele, H. J. Rosen, D. R. Schonhaut, W. J. Jagust, G. D. Rabinovici, Local and distant relationships between amyloid, tau and neurodegeneration in Alzheimer's Disease. *Neuroimage Clin.* **17**, 452–464 (2018).
7. I. M. Nasrallah, Y. J. Chen, M.-K. Hsieh, J. S. Phillips, K. Ternes, G. E. Stockbower, Y. Sheline, C. T. McMillan, M. Grossman, D. A. Wolk, ^{18}F-flortaucipir PET/MRI correlations in nonamnestic and amnestic variants of Alzheimer disease. *J. Nucl. Med.* **59**, 299–306 (2018).
8. R. Ossenkoppele, D. R. Schonhaut, M. Schöll, S. N. Lockhart, N. Ayakta, S. L. Baker, J. P. O'Neil, M. Janabi, A. Lazaris, A. Cantwell, J. Vogel, M. Santos, Z. A. Miller, B. M. Bettcher, K. A. Vossel, J. H. Kramer, M. L. Gorno-Tempini, B. L. Miller, W. J. Jagust, G. D. Rabinovici, Tau PET patterns mirror clinical and neuroanatomical variability in Alzheimer's disease. *Brain* **139**, 1551–1567 (2016).
9. J. Dronse, K. Fliessbach, G. N. Bischof, B. von Reutern, J. Faber, J. Hammes, G. Kuhnert, B. Neumaier, O. A. Onur, J. Kukolja, T. van Eimeren, F. Jessen, G. R. Fink, T. Klockgether, A. Drzezga, In vivo Patterns of tau pathology, amyloid-β burden, and neuronal dysfunction in clinical variants of Alzheimer's disease. *J. Alzheimers Dis.* **55**, 465–471 (2017).
10. A. Bejanin, D. R. Schonhaut, R. La Joie, J. H. Kramer, S. L. Baker, N. Sosa, N. Ayakta, A. Cantwell, M. Janabi, M. Lauriola, J. P. O'Neil, M. L. Gorno-Tempini, Z. A. Miller, H. J. Rosen, B. L. Miller, W. J. Jagust, G. D. Rabinovici, Tau pathology and neurodegeneration contribute to cognitive impairment in Alzheimer's disease. *Brain* **140**, 3286–3300 (2017).
11. M. J. Pontecorvo, M. D. Devous, M. Navitsky, M. Lu, S. Salloway, F. W. Schaerf, D. Jennings, A. K. Arora, A. McGeehan, N. C. Lim, H. Xiong, A. D. Joshi, A. Siderowf, M. A. Mintun; 18F-AV-1451-A05 investigators, Relationships between flortaucipir PET tau binding and amyloid burden, clinical diagnosis, age and cognition. *Brain* **140**, 748–763 (2017).
12. C. M. Firford, G. R. Ridgway, D. M. Cash, M. Modat, J. Nicholas, E. N. Manning, I. B. Malone, G. J. Biessels, S. Ourselin, O. T. Carmichael, M. J. Cardoso, J. Barnes; Alzheimer's Disease Neuroimaging Initiative, Patterns of progressive atrophy vary with age in Alzheimer's disease patients. *Neurobiol. Aging* **63**, 22–32 (2018).
13. H. Cho, S. Jeon, S. J. Kang, J.-M. Lee, J.-H. Lee, G. H. Kim, J. S. Shin, C. H. Kim, Y. Noh, K. Im, S. T. Kim, J. Chin, S. W. Seo, D. L. Na, Longitudinal changes of cortical thickness in early- versus late-onset Alzheimer's disease. *Neurobiol. Aging* **34**, 1921.e9–1921.e15 (2013).
14. D. Holland, R. S. Desikan, A. M. Dale, L. K. McEvoy; Alzheimer's Disease Neuroimaging Initiative, Rates of decline in Alzheimer disease decrease with age. *PLOS ONE* **7**, e42325 (2012).
15. L. E. M. Wisse, S. R. Das, C. Davatzikos, B. C. Dickerson, S. X. Xie, P. A. Yushkevich, D. A. Wolk, Defining SNAP by cross-sectional and longitudinal definitions of neurodegeneration. *Neuroimage Clin.* **18**, 407–412 (2018).
16. M. R. LaPoint, J. P. Chhatwal, J. Sepulcre, K. A. Johnson, R. A. Sperling, A. P. Schultz, The association between tau PET and retrospective cortical thinning in clinically normal elderly. *Neuroimage* **157**, 612–622 (2017).
17. S. R. Das, L. Xie, L. E. M. Wisse, R. Ittyerah, N. J. Tustison, B. C. Dickerson, P. A. Yushkevich, D. A. Wolk; Alzheimer's Disease Neuroimaging Initiative, Longitudinal and cross-sectional structural magnetic resonance imaging correlates of AV-1451 uptake. *Neurobiol. Aging* **66**, 49–58 (2018).
18. K. K. Leung, J. W. Bartlett, J. Barnes, E. N. Manning, S. Ourselin, N. C. Fox, Cerebral atrophy in mild cognitive impairment and Alzheimer disease: Rates and acceleration. *Neurology* **80**, 648–654 (2013).
19. M. R. Sabuncu, R. S. Desikan, J. Sepulcre, B. T. T. Yeo, H. Liu, N. J. Schmansky, M. Reuter, M. W. Weiner, R. L. Buckner, R. A. Sperling, B. Fischl; Alzheimer's Disease Neuroimaging Initiative, The dynamics of cortical and hippocampal atrophy in alzheimer disease. *Arch. Neurol.* **68**, 1040–1048 (2011).
20. J. M. Cedarbaum, M. Jaros, C. Hernandez, N. Coley, S. Andrieu, M. Grundman, B. Vellas; Alzheimer's Disease Neuroimaging Initiative, Rationale for use of the Clinical Dementia Rating Sum of Boxes as a primary outcome measure for Alzheimer's disease clinical trials. *Alzheimers Dement.* **9**, S45–S55 (2013).
21. M. L. Gorno-Tempini, A. E. Hillis, S. Weintraub, A. Kertesz, M. Mendez, S. F. Cappa, J. M. Ogar, J. D. Rohrer, S. Black, B. F. Boeve, F. Manes, N. F. Dronkers, R. Vandenberghe, K. Rascovsky, K. Patterson, B. L. Miller, D. S. Knopman, J. R. Hodges, M. M. Mesulam, M. Grossman, Classification of primary progressive aphasia and its variants. *Neurology* **76**, 1006–1014 (2011).
22. S. J. Crutch, J. M. Schott, G. D. Rabinovici, M. Murray, J. S. Snowden, W. M. van der Flier, B. C. Dickerson, R. Vandenberghe, S. Ahmed, T. H. Bak, B. F. Boeve, C. Butler, S. F. Cappa, M. Ceccaldi, L. C. de Souza, B. Dubois, O. Felician, D. Galasko, J. Graff-Radford, N. R. Graff-Radford, P. R. Hof, P. Krolak-Salmon, M. Lehmann, E. Magnin, M. F. Mendez, P. J. Nestor, C. U. Onyike, V. S. Pelak, Y. Pijnenburg, S. Primativo, M. N. Rossor, N. S. Ryan, P. Scheltens, T. J. Shakespeare, A. S. González, D. F. Tang-Wai, K. X. X. Yong, M. Carrillo, N. C. Fox; Alzheimer's Association ISTAART Atypical Alzheimer's Disease and Associated Syndromes Professional Interest Area, Consensus classification of posterior cortical atrophy. *Alzheimers Dement.* **13**, 870–884 (2017).
23. R. La Joie, A. Bejanin, A. M. Fagan, N. Ayakta, S. L. Baker, V. Bourakova, A. L. Boxer, J. Cha, A. Karydas, G. Jerome, A. Maass, A. Mensing, Z. A. Miller, J. P. O'Neil, J. Pham, H. J. Rosen, R. Tsai, A. V. Visani, B. L. Miller, W. J. Jagust, G. D. Rabinovici, Associations between [^{18}F] AV1451 tau PET and CSF measures of tau pathology in a clinical sample. *Neurology* **90**, e282–e290 (2018).
24. J. Ashburner, G. R. Ridgway, Symmetric diffeomorphic modeling of longitudinal structural MRI. *Front. Neurosci.* **6**, 197 (2013).
25. O. Potvin, L. Dieumegarde, S. Duchesne; Alzheimer's Disease Neuroimaging Initiative, Normative morphometric data for cerebral cortical areas over the lifetime of the adult human brain. *Neuroimage* **156**, 315–339 (2017).
26. A. Bejanin, R. La Joie, B. Landeau, S. Belliard, V. de La Sayette, F. Eustache, B. Desgranges, G. Chételat, Distinct interplay between atrophy and hypometabolism in Alzheimer's versus semantic dementia. *Cereb. Cortex* **29**, 1889–1899 (2019).
27. T. M. Harrison, R. La Joie, A. Maass, S. L. Baker, K. Swinnerton, L. Fenton, T. J. Mellinger, L. Edwards, J. Pham, B. L. Miller, G. D. Rabinovici, W. J. Jagust, Longitudinal tau accumulation and atrophy in aging and alzheimer disease. *Ann. Neurol.* **85**, 229–240 (2019).
28. L.-O. Wahlund, K. Blennow, Cerebrospinal fluid biomarkers for disease stage and intensity in cognitively impaired patients. *Neurosci. Lett.* **339**, 99–102 (2003).
29. W. J. P. Henneman, H. Vrenken, J. Barnes, I. C. Sluimer, N. A. Verwey, M. A. Blankenstein, M. Klein, N. C. Fox, P. Scheltens, F. Barkhof, W. M. van der Flier, Baseline CSF p-tau levels independently predict progression of hippocampal atrophy in Alzheimer disease. *Neurology* **73**, 935–940 (2009).
30. R. Tarawneh, D. Head, S. Allison, V. Buckles, A. M. Fagan, J. H. Ladenson, J. C. Morris, D. M. Holtzman, Cerebrospinal fluid markers of neurodegeneration and rates of brain atrophy in early Alzheimer disease. *JAMA Neurol.* **72**, 656–665 (2015).

31. A. M. Fjell, K. B. Walhovd, C. Fennema-Notestine, L. K. McEvoy, D. J. Hagler, D. Holland, J. B. Brewer, A. M. Dale; Alzheimer's Disease Neuroimaging Initiative, CSF Biomarkers in prediction of cerebral and clinical change in mild cognitive impairment and Alzheimer's disease. *J. Neurosci.* **30**, 2088–2101 (2010).
32. N. Schuff, N. Woerner, L. Boreta, T. Kornfield, L. M. Shaw, J. Q. Trojanowski, P. M. Thompson, C. R. Jack, M. W. Weiner; Alzheimer's Disease Neuroimaging Initiative, MRI of hippocampal volume loss in early Alzheimer's disease in relation to ApoE genotype and biomarkers. *Brain* **132**, 1067–1077 (2009).
33. J. D. Sluimer, F. H. Bouwman, H. Vrenken, M. A. Blankenstein, F. Barkhof, W. M. van der Flier, P. Scheltens, Whole-brain atrophy rate and CSF biomarker levels in MCI and AD: A longitudinal study. *Neurobiol. Aging* **31**, 758–764 (2010).
34. N. Mattsson, M. Schöll, O. Strandberg, R. Smith, S. Palmqvist, P. S. Insel, D. Hägerström, T. Ohlsson, H. Zetterberg, J. Jögi, K. Blennow, O. Hansson, ^{18}F-AV-1451 and CSF T-tau and P-tau as biomarkers in Alzheimer's disease. *EMBO Mol. Med.* **9**, 1212–1223 (2017).
35. J. P. Chhatwal, A. P. Schultz, G. A. Marshall, B. Boot, T. Gomez-Isla, J. Dumurgier, M. LaPoint, C. Scherzer, A. D. Roe, B. T. Hyman, R. A. Sperling, K. A. Johnson, Temporal T807 binding correlates with CSF tau and phospho-tau in normal elderly. *Neurology* **87**, 920–926 (2016).
36. J. M. Schott, J. W. Bartlett, J. Barnes, K. K. Leung, S. Ourselin, N. C. Fox, Reduced sample sizes for atrophy outcomes in Alzheimer's disease trials: Baseline adjustment. *Neurobiol. Aging* **31**, 1452–1462.e2 (2010).
37. D. M. Cash, J. D. Rohrer, N. S. Ryan, S. Ourselin, N. C. Fox, Imaging endpoints for clinical trials in Alzheimer's disease. *Alzheimers Res. Ther.* **6**, 87 (2014).
38. J. L. Whitwell, D. W. Dickson, M. E. Murray, S. D. Weigand, N. Tosakulwong, M. L. Senjem, D. S. Knopman, B. F. Boeve, J. E. Parisi, R. C. Petersen, C. R. Jack, K. A. Josephs, Neuroimaging correlates of pathologically defined subtypes of Alzheimer's disease: A case-control study. *Lancet Neurol.* **11**, 868–877 (2012).
39. X. Zhang, E. C. Mormino, N. Sun, R. A. Sperling, M. R. Sabuncu, B. T. T. Yeo; Alzheimer's Disease Neuroimaging Initiative, Bayesian model reveals latent atrophy factors with dissociable cognitive trajectories in Alzheimer's disease. *Proc. Natl. Acad. Sci. U.S.A.* **113**, E6535–E6544 (2016).
40. M. E. Murray, N. R. Graff-Radford, O. A. Ross, R. C. Petersen, R. Duara, D. W. Dickson, Neuropathologically defined subtypes of Alzheimer's disease with distinct clinical characteristics: A retrospective study. *Lancet Neurol.* **10**, 785–796 (2011).
41. B. A. Gutman, Y. Wang, I. Yanovsky, X. Hua, A. W. Toga, C. R. Jack, M. W. Weiner, P. M. Thompson, Empowering imaging biomarkers of Alzheimer's disease. *Neurobiol. Aging* **36** (Suppl. 1), S69–S80 (2015).
42. S. D. Edland, M. C. Ard, J. Sridhar, D. Cobia, A. Martersteck, M. M. Mesulam, E. J. Rogalski, Proof of concept demonstration of optimal composite MRI endpoints for clinical trials. *Alzheimers Dement.* **2**, 177–181 (2016).
43. R. La Joie, A. Perrotin, L. Barré, C. Hommet, F. Mézenge, M. Ibazizene, V. Camus, A. Abbas, B. Landeau, D. Guilloteau, V. de La Sayette, F. Eustache, B. Desgranges, G. Chételat, Region-specific hierarchy between atrophy, hypometabolism, and β-amyloid (Aβ) load in Alzheimer's disease dementia. *J. Neurosci.* **32**, 16265–16273 (2012).
44. G. Chételat, V. L. Villemagne, P. Bourgeat, K. E. Pike, G. Jones, D. Ames, K. A. Ellis, C. Szoeke, R. N. Martins, G. J. O'Keefe, O. Salvado, C. L. Masters, C. C. Rowe; Australian Imaging Biomarkers and Lifestyle Research Group, Relationship between atrophy and β-amyloid deposition in Alzheimer disease. *Ann. Neurol.* **67**, 317–324 (2010).
45. E. Falke, J. Nissanov, T. W. Mitchell, D. A. Bennett, J. Q. Trojanowski, S. E. Arnold, Subicular dendritic arborization in Alzheimer's disease correlates with neurofibrillary tangle density. *Am. J. Pathol.* **163**, 1615–1621 (2003).
46. T. Gómez-Isla, R. Hollister, H. West, S. Mui, J. H. Growdon, R. C. Petersen, J. E. Parisi, B. T. Hyman, Neuronal loss correlates with but exceeds neurofibrillary tangles in Alzheimer's disease. *Ann. Neurol.* **41**, 17–24 (1997).
47. A.-C. Dupont, B. Largeau, M. J. Santiago Ribeiro, D. Guilloteau, C. Tronel, N. Arlicot, Translocator protein-18 kDa (TSPO) Positron Emission Tomography (PET) imaging and its clinical impact in neurodegenerative diseases. *Int. J. Mol. Sci.* **18**, E785 (2017).
48. P. Bourgeat, G. Chételat, V. L. Villemagne, J. Fripp, P. Raniga, K. Pike, O. Acosta, C. Szoeke, S. Ourselin, D. Ames, K. A. Ellis, R. N. Martins, C. L. Masters, C. C. Rowe, O. Salvado, β-amyloid burden in the temporal neocortex is related to hippocampal atrophy in elderly subjects without dementia. *Neurology* **74**, 121–127 (2010).
49. E. Klupp, T. Grimmer, M. Tahmasian, C. Sorg, I. Yakushev, B. H. Yousefi, A. Drzezga, S. Förster, Prefrontal hypometabolism in Alzheimer disease is related to longitudinal amyloid accumulation in remote brain regions. *J. Nucl. Med.* **56**, 399–404 (2015).
50. K. A. Josephs, D. W. Dickson, N. Tosakulwong, S. D. Weigand, M. E. Murray, L. Petrucelli, A. M. Liesinger, M. L. Senjem, A. J. Spychalla, D. S. Knopman, J. E. Parisi, R. C. Petersen, C. R. Jack, J. L. Whitwell, Rates of hippocampal atrophy and presence of post-mortem TDP-43 in patients with Alzheimer's disease: A longitudinal retrospective study. *Lancet Neurol.* **16**, 917–924 (2017).
51. J. L. Whitwell, J. Graff-Radford, N. Tosakulwong, S. D. Weigand, M. M. Machulda, M. L. Senjem, A. J. Spychalla, P. Vemuri, D. T. Jones, D. A. Drubach, D. S. Knopman, B. F. Boeve, N. Ertekin-Taner, R. C. Petersen, V. J. Lowe, C. R. Jack, K. A. Josephs, Imaging correlations of tau, amyloid, metabolism, and atrophy in typical and atypical Alzheimer's disease. *Alzheimers Dement.* **14**, 1005–1014 (2018).
52. A. A. J. Gerritsen, C. Bakker, F. R. J. Verhey, M. E. de Vugt, R. J. F. Melis, R. T. C. M. Koopmans, 4C study team, Prevalence of comorbidity in patients with young-onset Alzheimer disease compared with late-onset: A comparative cohort study. *J. Am. Med. Dir. Assoc.* **17**, 318–323 (2016).
53. G. D. Rabinovici, M. C. Carrillo, M. Forman, S. DeSanti, D. S. Miller, N. Kozauer, R. C. Petersen, C. Randolph, D. S. Knopman, E. E. Smith, M. Isaac, N. Mattsson, L. J. Bain, J. A. Hendrix, J. R. Sims, Multiple comorbid neuropathologies in the setting of Alzheimer's disease neuropathology and implications for drug development. *Alzheimers Dement.* **3**, 83–91 (2017).
54. B. D. James, D. A. Bennett, P. A. Boyle, S. Leurgans, J. A. Schneider, Dementia from Alzheimer disease and mixed pathologies in the oldest old. *JAMA* **307**, 1798–1800 (2012).
55. M. Marquié, E. E. Verwer, A. C. Meltzer, S. J. W. Kim, C. Agüero, J. Gonzalez, S. J. Makaretz, M. Siao Tick Chong, P. Ramanan, A. C. Amaral, M. D. Normandin, C. R. Vanderburg, S. N. Gomperts, K. A. Johnson, M. P. Frosch, T. Gómez-Isla, Lessons learned about [F-18]-AV-1451 off-target binding from an autopsy-confirmed Parkinson's case. *Acta Neuropathol. Commun.* **5**, 75 (2017).
56. K. Sander, T. Lashley, P. Gami, T. Gendron, M. F. Lythgoe, J. D. Rohrer, J. M. Schott, T. Revesz, N. C. Fox, E. Årstad, Characterization of tau positron emission tomography tracer [^{18}F]AV-1451 binding to postmortem tissue in Alzheimer's disease, primary tauopathies, and other dementias. *Alzheimers Dement.* **12**, 1116–1124 (2016).
57. J. Y. Choi, H. Cho, S. J. Ahn, J. H. Lee, Y. H. Ryu, M. S. Lee, C. H. Lyoo, Off-target ^{18}F-AV-1451 binding in the basal ganglia correlates with age-related iron accumulation. *J. Nucl. Med.* **59**, 117–120 (2018).
58. S. L. Baker, A. Maass, W. J. Jagust, Considerations and code for partial volume correcting [^{18}F]-AV-1451 tau PET data. *Data Brief* **15**, 648–657 (2017).
59. S. N. Lockhart, N. Ayakta, J. R. Winer, R. La Joie, G. D. Rabinovici, W. J. Jagust, Elevated ^{18}F-AV-1451 PET tracer uptake detected in incidental imaging findings. *Neurology* **88**, 1095–1097 (2017).
60. R. M. Tsai, A. Bejanin, O. Lesman-Segev, R. LaJoie, A. Visani, V. Bourakova, J. P. O'Neil, M. Janabi, S. Baker, S. E. Lee, D. C. Perry, L. Bajorek, A. Karydas, S. Spina, L. T. Grinberg, W. W. Seeley, E. M. Ramos, G. Coppola, M. L. Gorno-Tempini, B. L. Miller, H. J. Rosen, W. Jagust, A. L. Boxer, G. D. Rabinovici, ^{18}F-flortaucipir (AV-1451) tau PET in frontotemporal dementia syndromes. *Alzheimers Res. Ther.* **11**, 13 (2019).
61. L. Bakota, R. Brandt, Tau biology and tau-directed therapies for Alzheimer's disease. *Drugs* **76**, 301–313 (2016).
62. G. M. McKhann, D. S. Knopman, H. Chertkow, B. T. Hyman, C. R. Jack Jr., C. H. Kawas, W. E. Klunk, W. J. Koroshetz, J. J. Manly, R. Mayeux, R. C. Mohs, J. C. Morris, M. N. Rossor, P. Scheltens, M. C. Carrillo, B. Thies, S. Weintraub, C. H. Phelps, The diagnosis of dementia due to Alzheimer's disease: Recommendations from the National Institute on Aging-Alzheimer's Association workgroups on diagnostic guidelines for Alzheimer's disease. *Alzheimers Dement.* **7**, 263–269 (2011).
63. M. S. Albert, S. T. DeKosky, D. Dickson, B. Dubois, H. H. Feldman, N. C. Fox, A. Gamst, D. M. Holtzman, W. J. Jagust, R. C. Petersen, P. J. Snyder, M. C. Carrillo, B. Thies, C. H. Phelps, The diagnosis of mild cognitive impairment due to Alzheimer's disease: Recommendations from the National Institute on Aging-Alzheimer's Association workgroups on diagnostic guidelines for Alzheimer's disease. *Alzheimers Dement.* **7**, 270–279 (2011).
64. G. D. Rabinovici, H. J. Rosen, A. Alkalay, J. Kornak, A. J. Furst, N. Agarwal, E. C. Mormino, J. P. O'Neil, M. Janabi, A. Karydas, M. E. Growdon, J. Y. Jang, E. J. Huang, S. J. Dearmond, J. Q. Trojanowski, L. T. Grinberg, M. L. Gorno-Tempini, W. W. Seeley, B. L. Miller, W. J. Jagust, Amyloid vs FDG-PET in the differential diagnosis of AD and FTLD. *Neurology* **77**, 2034–2042 (2011).
65. J. Diedrichsen, J. H. Balsters, J. Flavell, E. Cussans, N. Ramnani, A probabilistic MR atlas of the human cerebellum. *Neuroimage* **46**, 39–46 (2009).
66. A. Maass, S. Landau, S. L. Baker, A. Horng, S. N. Lockhart, R. La Joie, G. D. Rabinovici, W. J. Jagust; Alzheimer's Disease Neuroimaging Initiative, Comparison of multiple tau-PET measures as biomarkers in aging and Alzheimer's disease. *Neuroimage* **157**, 448–463 (2017).
67. A. Hammers, R. Allom, M. J. Koepp, S. L. Free, R. Myers, L. Lemieux, T. N. Mitchell, D. J. Brooks, J. S. Duncan, Three-dimensional maximum probability atlas of the human brain, with particular reference to the temporal lobe. *Hum. Brain Mapp.* **19**, 224–247 (2003).
68. H. Girard, O. Potvin, S. Nugent, C. Dallaire-Théroux, S. Cunnane, S. Duchesne; Alzheimer's Disease Neuroimaging Initiative, Faster progression from MCI to probable AD for carriers of a single-nucleotide polymorphism associated with type 2 diabetes. *Neurobiol. Aging* **64**, 157.e11–157.e17 (2018).
69. C. R. Pernet, R. Wilcox, G. A. Rousselet, Robust correlation analyses: False positive and power validation using a new open source matlab toolbox. *Front. Psychol.* **3**, 606 (2012).

70. M. Xia, J. Wang, Y. He, BrainNet Viewer: A network visualization tool for human brain connectomics. *PLOS ONE* **8**, e68910 (2013).

Acknowledgments: We thank the patients and their caregivers for their participation in the study. Avid Radiopharmaceuticals enabled use of the [^{18}F]flortaucipir tracer by providing precursor but did not provide direct funding and was not involved in data analysis or interpretation. **Funding:** Alzheimer's Association (AARF-16-443577 to R.L.J.), National Institute on Aging grants (R01-AG045611 to G.D.R.; P50-AG023501 to B.L.M. and G.D.R.; P01-AG19724 to W.J.J., B.L.M., and G.D.R.), Tau Consortium (to G.D.R. and W.J.J.), and State of California Department of Health Services Alzheimer's Disease Research Centre of California grant (04-33516 to B.L.M.). **Author contributions:** Study conceptualization: R.L.J. and G.D.R.; data acquisition and quality control: R.L.J., A.V.V., S.L.B., V.B., K.C., L.E., M.J., O.H.L.-S., Z.A.M., D.C.P., J.P.O., J.P., J.C.R., H.J.R., R.M.T., B.L.M., W.J.J., and G.D.R.; data processing and methodology: R.L.J., A.V.V., S.L.B., J.A.B., V.B., J.C., L.E., L.I., O.H.L.-S., and W.W.S.; data analysis: R.L.J.; writing the original draft: R.L.J.; reviewing and editing manuscript: all authors; supervision: G.D.R.; project administration and resources: K.C.; funding acquisition: R.L.J., B.L.M., W.J.J., and G.D.R. **Competing interests:** D.C.P. receives support from the NIH (K23AG045289). J.C.R. receives support from the NIH (R01 AG038791 PI, Adam Boxer) and travel funds from Eli Lilly. S.L.B. consults for Genentech. W.W.S. receives research support from NIH/NIA and has received consulting fees from Merck Inc., Biogen Idec, and Bristol-Myers Squibb. H.J.R. receives research support from the NIH/National Institute on Aging, RO1 AG032306 (PI), PO1 AG019724 (Core leader), AG045333 (PI), and AG023501 (Core leader). R.M.T. receives research support from the University of California. R.M.T. also consulted for ExpertConnect and Grifols. B.L.M. receives research support from the NIH/NIA and the Centers for Medicare & Medicaid Services (CMS) as grants for the Memory and Aging Center. As an additional disclosure, B.L.M. serves as Medical Director for the John Douglas French Foundation; Scientific Director for the Tau Consortium; Director/Medical Advisory Board of the Larry L. Hillblom Foundation; Scientific Advisory Board Member for the National Institute for Health Research Cambridge Biomedical Research Centre and its subunit, the Biomedical Research Unit in Dementia (UK); and Board Member for the American Brain Foundation (ABF). W.J.J. has served as a consultant to BioClinica, Genentech, and Novartis Pharmaceuticals. G.D.R. receives research support from Avid Radiopharmaceuticals, GE Healthcare, and Life Molecular Imaging and has received consulting fees or speaking honoraria from Axon Neurosciences, Roche, Eisai, Genentech, Merck. The other authors declare that they have no competing interests. **Data and materials availability:** Most data associated with this study are available in the main text, supplementary data file, or on neurovault for group-level voxelwise images (https://neurovault.org/collections/WLDODMCY/). Individual MRI and PET images data will be shared with external investigators upon submission of a proposal and under a data transfer agreement.

Submitted 3 August 2018
Resubmitted 13 September 2019
Accepted 13 November 2019
Published 1 January 2020
10.1126/scitranslmed.aau5732

Citation: R. La Joie, A. V. Visani, S. L. Baker, J. A. Brown, V. Bourakova, J. Cha, K. Chaudhary, L. Edwards, L. Iaccarino, M. Janabi, O. H. Lesman-Segev, Z. A. Miller, D. C. Perry, J. P. O'Neil, J. Pham, J. C. Rojas, H. J. Rosen, W. W. Seeley, R. M. Tsai, B. L. Miller, W. J. Jagust, G. D. Rabinovici, Prospective longitudinal atrophy in Alzheimer's disease correlates with the intensity and topography of baseline tau-PET. *Sci. Transl. Med.* **12**, eaau5732 (2020).

Science Translational Medicine

Prospective longitudinal atrophy in Alzheimer's disease correlates with the intensity and topography of baseline tau-PET

Renaud La Joie, Adrienne V. Visani, Suzanne L. Baker, Jesse A. Brown, Viktoriya Bourakova, Jungho Cha, Kiran Chaudhary, Lauren Edwards, Leonardo Iaccarino, Mustafa Janabi, Orit H. Lesman-Segev, Zachary A. Miller, David C. Perry, James P. O'Neil, Julie Pham, Julio C. Rojas, Howard J. Rosen, William W. Seeley, Richard M. Tsai, Bruce L. Miller, William J. Jagust and Gil D. Rabinovici

Sci Transl Med **12**, eaau5732.
DOI: 10.1126/scitranslmed.aau5732

Predictive PET

Understanding the dynamic of the two major hallmark of Alzheimer's disease (AD), tau protein and β-amyloid, in the brain could allow better disease management. The use of positron emission tomography (PET) with specific radiotracers allows the visualization of tau-containing neurofibrillary tangles and β-amyloid plaques in vivo. Now, La Joie *et al.* performed longitudinal analysis of tau-PET and β-amyloid–PET in 32 patients with AD starting at early disease stage and correlated the signal with brain atrophy at later stages. In this cohort, tau-PET, but not β-amyloid–PET, signal could predict brain atrophy at later stages. Tau-PET might be useful for predicting disease progression and for designing and evaluating new therapies.